nature chemistry

ARTICLES

PUBLISHED ONLINE: 30 JUNE 2013 | DOI: 10.1038/NCHEM.1695

Single-molecule interrogation of a bacterial sugar transporter allows the discovery of an extracellular inhibitor

Lingbing Kong, Leon Harrington, Qiuhong Li†, Stephen Cheley†, Benjamin G. Davis* and Hagan Bayley*

Capsular polysaccharides form the outermost protective layer around many Gram-negative bacteria. Antibiotics aimed directly at weakening this layer are not yet available. In pathogenic *Escherichia coli* E69, a protein, Wza, forms a pore in the outer membrane that transports K30 capsular polysaccharide from its site of synthesis to the outside of the cell. This therefore represents a prospective antibiotic target. Here we test a variety of grommet-like mimics of K30 capsular polysaccharide on wild-type Wza and on mutant open forms of the pore by electrical recording in planar lipid bilayers. The most effective glycomimetic was the unnatural cyclic octasaccharide octakis(6-deoxy-6-amino)cyclomaltooctaose ($am_8\gamma CD$), which blocks the α-helix barrel of Wza, a site that is directly accessible from the external medium. This glycomimetic inhibited K30 polysaccharide transport in live *E. coli* E69. With the protective outer membrane disrupted, the bacteria can be recognized and killed by the human immune system.

By 2004, over 70% of pathogenic bacteria had acquired resistance to at least one commercially available antibiotic[1]. Recent years have seen an alarming trend towards combined resistance[2]. As a consequence, over the last seven years, the pharmaceutical industry worldwide has spent more than 30 billion dollars on the development of new antibiotics. However, as microorganisms continue to acquire resistance, the value of this investment and the effectiveness of drugs aimed at current targets are diminishing[3]. Accordingly, antibiotics that act on new targets and developing superior strategies for screening their effectiveness are of central importance.

High-molecular-weight capsular polysaccharides (CPSs) form the outermost protective layer of many Gram-negative bacteria[4–6]. Antibiotics aimed directly at weakening the CPS layer are not yet available, although antimicrobial peptides, salicylate and bismuth compounds inhibit CPS production[7,8]. CPS offers a defence against environmental factors, including attack by the immune system of the host[9,10]. The outer membrane of Gram-negative bacteria has an underlying second protective layer of lipopolysaccharides (LPSs)[4,11]. There are approximately 80 different K-antigens (CPS) and 170 O-antigens (LPS) found in different *Escherichia coli* strains. Of the CPS variants, groups 1 and 4 share the same assembly system, which includes the protein pore Wza[10]. Several other bacterial species make use of a transport system that includes Wza, including *Klebsiella pneumonia*, *Actinobacillus suis* and *Bordetella bronchiseptica*. X-ray analysis of Wza reveals a structure that includes a novel eight-helix barrel[12]. The bulk of the Wza octamer, which contains a spacious central lumen, has been deduced to lie in the periplasm, with the helix barrel spanning the outer membrane (Fig. 1a).

Here, we screen Wza, by carrying out single-channel electrical recording in planar lipid bilayers, for blockers that act when applied to the extracellular aspect of the pore (Supplementary Fig. S1). Screening was facilitated by exploiting open forms of Wza prepared by mutagenesis. The most effective glycomimetic blocker discovered by this approach, octakis(6-deoxy-6-amino)-cyclomaltooctaose ($am_8\gamma CD$, **13**), acts on living bacteria to cause loss of CPS, which in turn exposes the bacteria to immune attack.

Results

Engineering an open form of Wza. The X-ray structure[12] of wild-type (WT) Wza (PDB: 2J58) suggested a very narrow opening, ~8 Å in diameter, from the medium to the pore lumen, at the end of the protein that lies closest to the peptidoglycan layer in the intact bacterium (Fig. 1). A conductance histogram of the WT pore from *E. coli* revealed sequential insertion events yielding active pores with a mean single channel current of 1.9 ± 0.2 pA ($n = 37$) at +100 mV in 2 M KCl, corresponding to a unitary conductance of 19 ± 2 pS ($n = 37$) (Supplementary Fig. S2).

Having established pore-forming activity from Wza extracted from bacteria, we next tested WT Wza expressed in a cell-free system. After *in vitro* transcription and translation (IVTT)[13,14], the octamer, which formed spontaneously, was purified by SDS-polyacrylamide electrophoresis (SDS-PAGE; Fig. 2a, lane 1). The *I–V* curves of WT Wza octamers extracted from *E. coli* and prepared by IVTT were very similar (Supplementary Fig. S3). The WT Wza channel did not show significant ion selectivity (Supplementary Figs S4–S6).

We next sought mutant pores of higher unitary conductance that would mimic the state found in living bacteria, where Wza is held open by the inner membrane protein Wzc[15]. Examination of the crystal structure[12] suggested replacement of tyrosine residues at position 110, which line the narrowest region of the pore lumen (Fig. 1b), with glycine. In addition, cysteine residues were

Department of Chemistry, University of Oxford, Chemical Research Laboratory, Mansfield Road, Oxford OX1 3TA, UK; †Present address: Chester Beatty Laboratories, Institute of Cancer Research, Division of Structural Biology, 237 Fulham Road, London SW3 6JB, UK (Q.L.); Alberta Diabetes Institute, Department of Pharmacology, Li Ka Shing Centre, University of Alberta, Edmonton, Alberta T5V 1K6, Canada (S.C.). *e-mail: hagan.bayley@chem.ox.ac.uk; ben.davis@chem.ox.ac.uk

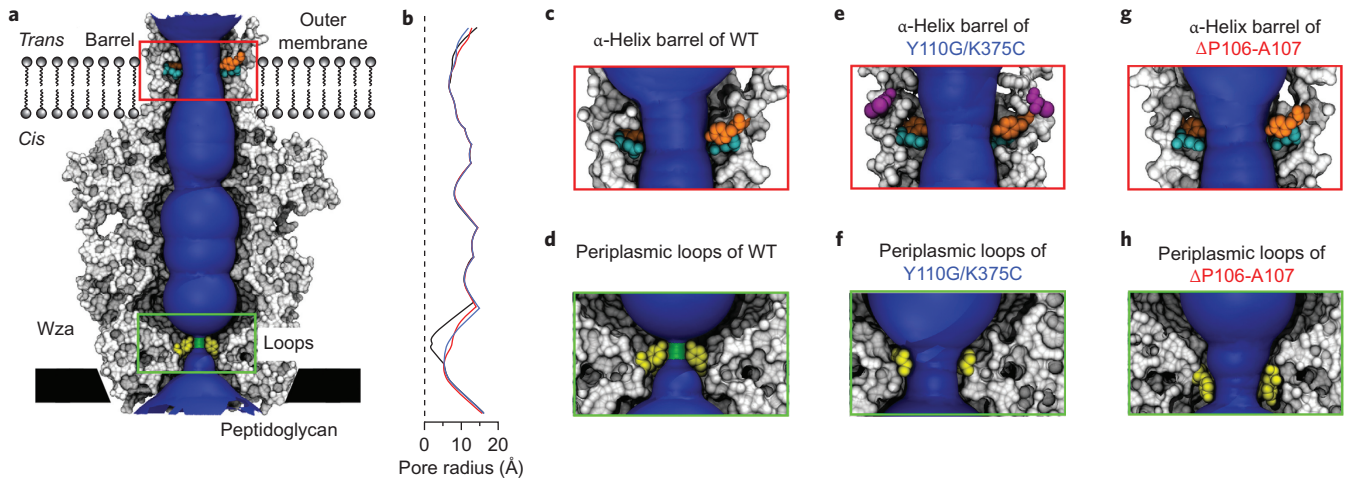

Figure 1 | Models of sections of WT Wza, Wza Y110G/K375C and Wza ΔP106-A107 and their pore radii. The models were generated with MODELLER[24] v9.6 by using the WT Wza crystal structure (PDB: 2J58) as a template. The pore radii were determined with HOLE[49] and visualized in VMD[50]. The blue surface represents regions of the pore where the radius is >2.30 Å, while green indicates regions where the passage has narrowed to a radius between 1.15 Å and 2.30 Å. **a**, WT Wza. Tyr-373, orange; Glu-369, cyan; Tyr-110, yellow. **b**, Pore radii of WT Wza (black), Y110G/K375C (blue) and ΔP106-A107 (red). **c**, α-Helix barrel of WT Wza. Tyr-373, orange; Glu-369, cyan. **d**, Periplasmic loops of WT Wza. Tyr-110, yellow. **e**, α-Helix barrel of Wza Y110G/K375C. Tyr-373, orange; Glu-369, cyan; Cys-375, purple. **f**, Periplasmic loops of Wza Y110G/K375C. Gly-110, yellow. **g**, α-Helix barrel of Wza ΔP106-A107. Tyr-371, orange; Glu-367, cyan. **h**, Periplasmic loops of Wza ΔP106-A107. Tyr-108, yellow.

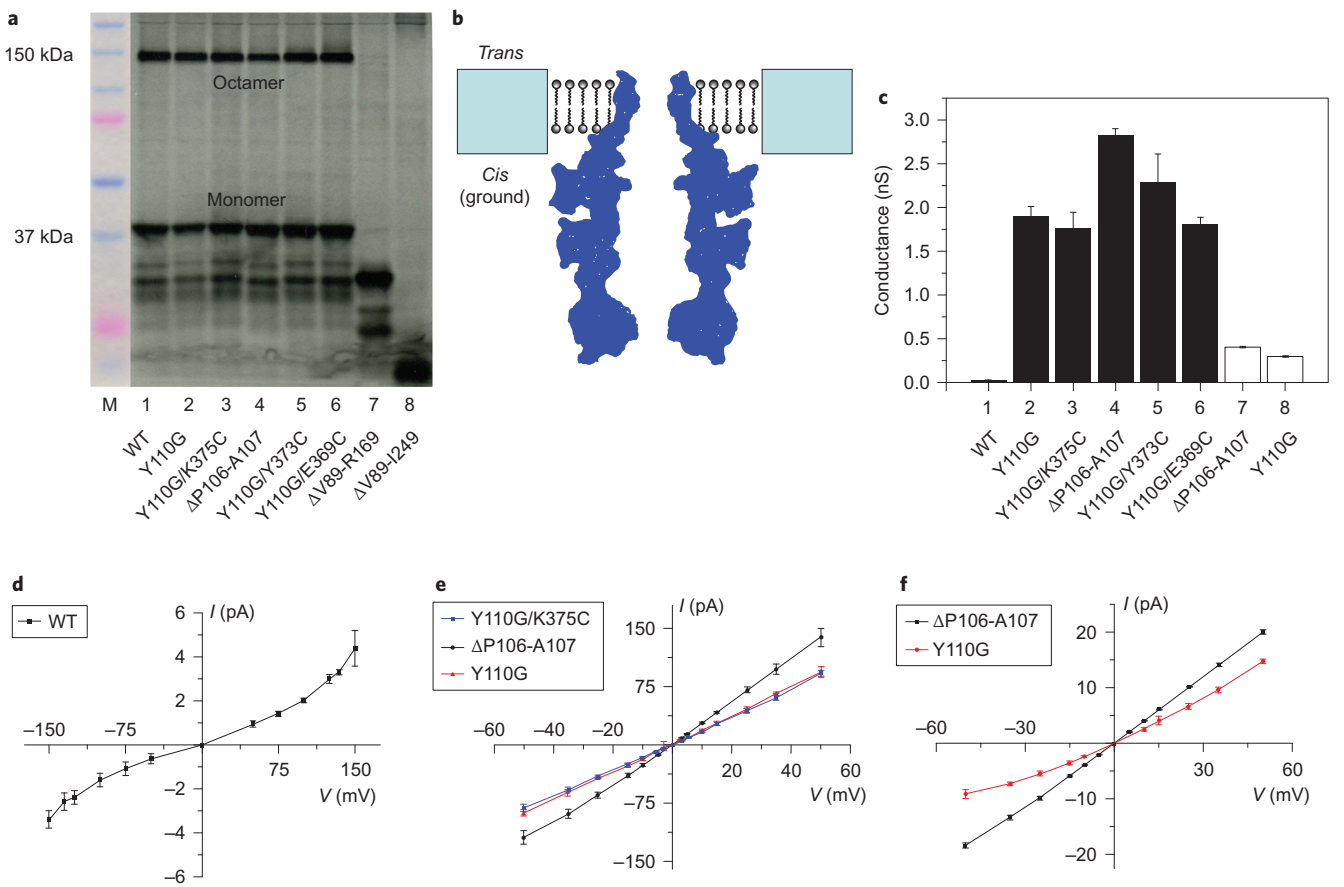

Figure 2 | Preparation and electrical properties of WT Wza and Wza mutants. a, Radiolabelled Wza proteins were expressed by IVTT and subjected to SDS-PAGE. An autoradiograph is shown, with markers alongside. M, protein markers. **b**, Setup for single-channel recording with the Wza pore in a planar bilayer system. The protein is inserted into the bilayer from the *cis* chamber (ground). **c**, Unitary conductance values for WT and mutant Wza octamers in KCl buffers (for numerical values see Supplementary Fig. S14). Black filled bars indicate values in 2 M KCl buffer; open bars indicate values in 300 mM KCl buffer. **d**, *I–V* curve for WT Wza in 2 M KCl, 5 mM HEPES, 100 μM EDTA, 200 μM DTT, pH 7.5 ($n = 3$). **e**, *I–V* curves of mutants Y110G (red, $n = 3$), Y110G/K375C (blue, $n = 3$) and ΔP106-A107 (black, $n = 3$) in 2 M KCl, 5 mM HEPES, 100 μM EDTA, 200 μM DTT, pH 7.5. **f**, *I–V* curves of mutants Y110G (red, $n = 3$) and ΔP106-A107 (black, $n = 3$) in 300 mM KCl, 5 mM HEPES, pH 7.5. Mean values (±s.d.) from at least three independent experiments are shown in **c–f**.

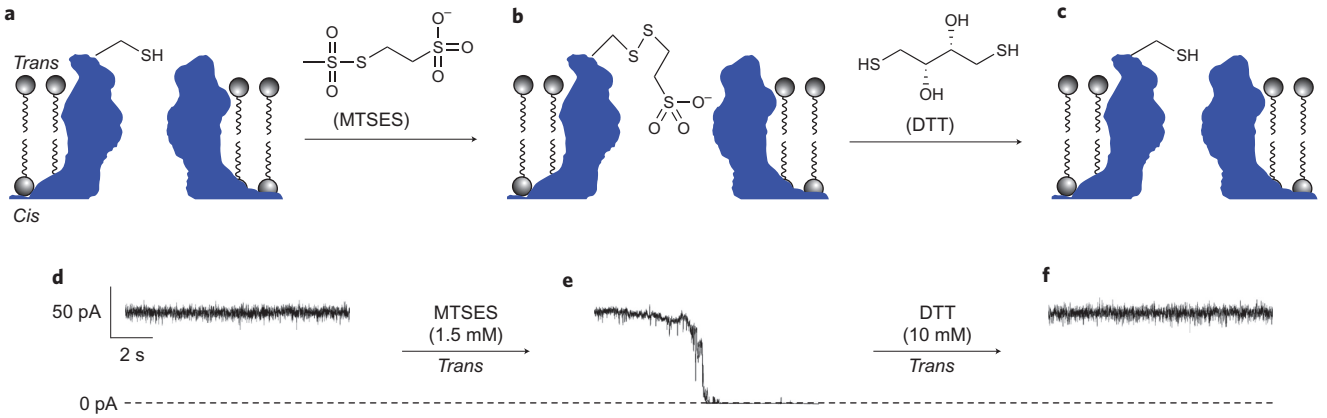

Figure 3 | Reaction of the Wza mutant Y110G/K375C with MTSES. The buffers are 2 M KCl, 5 mM HEPES, 100 μM EDTA, 200 μM DTT, pH 7.5. **a–c**, Schematic showing reaction of the eight cysteine residues of Y110G/K375C with MTSES and cleavage of the disulfide bonds of the MTSES adducts by DTT. **d–f**, Single-channel recording traces of the reaction of Y110G/K375C with MTSES (1.5 mM, *trans*) followed by treatment with DTT (10 mM, *trans*) at +50 mV. The sampling rate is 5 kHz.

introduced at position 375 at the entrance of the α-helix barrel (Y110G/K375C, Fig. 1e) so that it could be confirmed, by reversible blockade with a thiol-selective protein modification reagent[16,17], that the measured current was a result of ion flow through the Wza pore. The narrowest constriction within WT Wza has a diameter of 3.7 Å, whereas the narrowest constriction within Y110G/K375C, which remains at the same site, has a diameter of 10.5 Å (Fig. 1f).

By observing stepwise insertion events at +50 mV, the current carried by the octameric Y110G/K375C pore (Fig. 2a, lane 3) was determined to be +88±10 pA in 2 M KCl, (n = 31, Supplementary Fig. S7), 1,800±200 pS (n = 31). The single-channel I–V curve (Fig. 2e, blue) shows that the pore is stable over a range of potentials. In addition, the reaction between the eight Cys-375 residues and (2-sulfonatoethyl)methanethiosulfonate (MTSES)[18], added to the *trans* compartment (Fig. 2b), confirmed that the current passes through the eight-helix barrel. The current was reduced to zero, presumably by the formation of mixed disulfide bonds with Cys-375 (Fig. 3a→b or d→e), and the pore was re-opened by the addition of excess reduced dithiothreitol (*trans*) (Fig. 3b→c or e→f).

Screening for Wza blockers. Single-channel recording has proven effective in searches for channel blockers, including, as in the present case, blockers for large pores[19–21]. In an early example, we showed that cyclodextrins block the staphylococcal α-haemolysin pore[22]. Structural studies[20] have shown that the cyclodextrins act as 'grommets', with their axis of rotational symmetry aligned with that of the pore[20,23]. We therefore reasoned that cyclodextrins and related structures might block Wza, especially if the blocker and target were matched in symmetry[20,23], although we noted that the previous examples mostly involved transmembrane β-barrels. We further argued that K30 CPS, during transport through Wza, might adopt a helical structure[24–30] that would be guided by an external display of both hydrogen-bonding capacity and charge along its loose 'cylindrical surface' (see Supplementary Fig. S8 for a model). Therefore, cyclic oligosaccharides (cyclodextrins) and other sugar-like (glycomimetic) compounds capable of mimicking cross-sections of this 'saccharidic cylinder' (estimated diameter of 17–21 Å, Supplementary Fig. S8) would be adept at binding within Wza by exploiting charge–charge and hydrogen bonding interactions at the narrowest region of Wza within the alpha helix barrel (Fig. 4a,b). Based on both the earlier examples of β-barrel grommets and this putative, 'sectional glycomimicry', we postulated that Wza might have a binding site, as yet undiscovered, that we could target with cyclic glycomimetics (Fig. 4b).

We examined a panel of compounds by planar bilayer recording with WT Wza and Y110G/K375C (compounds 1–16, Supplementary Fig. S9, Supplementary Table S1). Suggesting a selective interaction, only two compounds elicited clear current blockades: cyclic heptasaccharide am$_7$βCD (**10**, Fig. 4c) and cyclic octasaccharide am$_8$γCD (**13**, Fig. 4c).

Am$_7$βCD **10** (*trans*) blocked the WT Wza pore with K_d = 13±7 mM (n = 3) in 2 M KCl, at +75 mV (Fig. 5a). The interaction between WT Wza and am$_8$γCD **13** was not detectable (Supplementary Fig. S10). Am$_7$βCD **10** also interacted with the Y110G/K375C pore with K_d = 2.1±0.5 mM (+75 mV, n = 3) (Fig. 5b). The K_d values with Y110G/K375C at a low applied potential (+3 mV) in 2 M KCl were 2.9±1.8 mM (n = 3) for Y110G/K375C·**10** and 13±2 μM (n = 3) for Y110G/K375C·**13**.

The promising activity of am$_8$γCD **13**, more than 200-fold more potent than am$_7$βCD **10** with Y110G/K375C, was examined in greater detail. Notably, the affinity of am$_8$γCD **13** was voltage-dependent (Fig. 5h, blue), dropping from 13±2 μM (n = 3) at +3 mV to 220±14 μM (n = 3) at +35 mV for Y110G/K375C. The affinity of am$_7$βCD **10** varied much less with voltage. Importantly, despite its voltage dependency, the binding of am$_8$γCD **13** to Y110G/K375C was similarly strong at both low positive and low negative potentials (+3 mV and −3 mV, for example, Fig. 5c,h). This is significant because the potential across the outer membrane of *E. coli* is low, <7 mV (inside negative) in >300 mM NaCl[31–33], and experiments at high potentials are therefore less relevant to live cells.

To better understand the interaction, the kinetics of am$_8$γCD **13** binding to the Y110G/K375C pore were investigated. k_{off} values were obtained over a range of potentials (Supplementary Fig. S11a,b). Notably, τ_{off} dropped dramatically at >+15 mV, suggesting that am$_8$γCD **13** translocates through the pore when driven by higher potentials. Dissociation constants (K_d) for Y110G/K375C·**13** were derived from the k_{off} and k_{on} (Supplementary Fig. S11c) values. The lowest value of K_d was 6.8±1.0 μM (n = 3) at +10 mV (Fig. 5h, blue). Log K_d displayed a linear correlation with the applied potential, both above and below the +10 mV threshold, consistent with Woodhull's model for voltage-dependent binding of a charged channel blocker[34,35].

Blockade of Wza with an unaltered α-helix barrel. We next examined the blocking of Wza pores with various mutations, to discover the am$_8$γCD **13** binding site. The ΔV89-R169 and

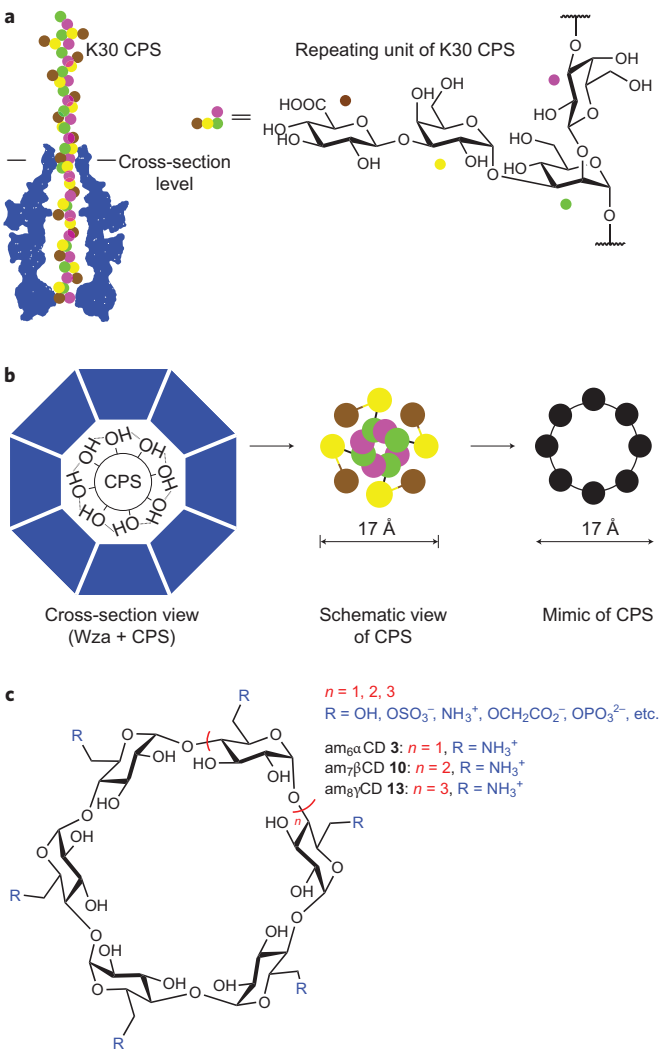

Figure 4 | Screening of blockers against WT Wza and Wza mutants. **a**, Transport of K30 CPS through the Wza pore. Sugar residues in the repeating tetrasaccharide unit are represented by the coloured spheres (green, α-D-mannosyl; magenta, β-D-galactosyl; yellow, α-D-galactosyl; brown, β-D-glucuronyl). **b**, Left: cross-section of Wza containing the CPS 'saccharidic cylinder' at the cross-sectional level highlighted in **a**. Middle: schematic view looking down the modelled CPS helix (Supplementary Fig. S8) at the same cross-sectional level, showing the relative positions of sugar residues (using the colour scheme from **a**). Right: size and symmetry of grommet-like, cyclic glycomimetics (for example, based on γ-cyclodextrin scaffolds) as cross-sectional mimics of CPS. **c**, Structures of a selection of the glycomimetic compounds used for screening. Compounds $am_6αCD$ (**3**), $am_7βCD$ (**10**) and $am_8γCD$ (**13**) are highlighted. See Supplementary Table S1 for full details of the additional compounds that were tested.

ΔV89-I249 mutants (deletions of the entire domains 1 or domains 1 and 2, respectively) could be expressed as monomers but did not self-assemble (Fig. 2a, lanes 7 and 8) and so were not examined further. Of the mutants that did form octamers, ΔP106-A107 had the highest unitary conductance (2.8 ± 0.2 nS, $n = 3$) and was the least prone to gating in 2 M KCl (*I–V* curve; Fig. 2e, black). ΔP106-A107 was also blocked by $am_8γCD$ **13** (Fig. 5f), and the log K_d–*V* curve (Fig. 5h, black) closely resembled that of Y110G/K375C (Fig. 5h, blue). Y110G was also examined (Fig. 5e, left; Fig. 2e, red). The K_d for Y110G·**13** in 2 M KCl was also close to the value for ΔP106-A107 (Supplementary Table S3) and the other mutants with unaltered α-helix barrels. The lifetimes of the complexes between $am_8γCD$ **13** and the mutant Wza pores with unaltered barrels were distributed as single exponential functions, suggesting a single binding site for **13** within the pore lumen (Supplementary Fig. S12).

Interaction of blocker with proteolytically cleaved WT Wza. Our results demonstrate that $am_8γCD$ **13** blocks Wza pores with intact α-helix barrels, suggesting the barrel as a possible binding site. The outer diameter of $am_8γCD$ **13** is ~17 Å, similar to the internal diameter (17 Å) of the α-helix barrel of Wza. However, the periplasmic (*cis*) end of the protein, which lies close to the peptidoglycan layer in cells, also has a narrow entrance. To distinguish between these two sites, we digested the *cis* end of the pore with proteinase K, after it had inserted into a planar bilayer. After digestion, WT Wza yielded a highly conductive pore in 2 M KCl, with rare current spikes (Fig. 6b). The current at +100 mV was 711 ± 46 pA ($n = 7$, unitary conductance = 7,110 ± 460 pS). Despite the loss of the *cis* end, $am_8γCD$ **13** (*trans*) produced current blockades. The overall K_d (all levels) of cleaved WT Wza·**13** was 57 ± 22 nM ($n = 3$) at +100 mV. The continued ability of WT Wza·**13** to block the proteolysed pore implicated the α-helix barrel in binding.

Identification of amino acids involved in blocker binding. To further define the binding site, two additional mutant pores were prepared that had cysteine side chains that project into the lumen of the α-helix barrel: Y110G/Y373C and Y110G/E369C (Fig. 6e,g). The *I–V* curves of the Y110G/Y373C and Y110G/E369C pores (Supplementary Fig. S13) suggested that, like their progenitor Y110G, both were more open at the periplasmic end by comparison with WT Wza. The addition of MTSES closed these pores, consistent with the presence of cysteine residues within the lumen. However, the Y110G/Y373C pore interacted only weakly with $am_8γCD$ **13** (*trans*, Fig. 6f, right) with a K_d value of 1.0 ± 0.3 mM (+3 mV, $n = 3$) (Supplementary Table S3), suggesting that the Tyr-373 residues are required for tight binding of the blocker. Moreover, Y110G/E369C did not interact at all with $am_8γCD$ **13**, even at a high concentration (200 μM, *trans*, Fig. 6h, right), so the Glu-369 residues within the α-helix barrel are critical for the binding of $am_8γCD$ **13**. Together, these results pinpoint the blocker binding site within the α-helix barrel.

To further investigate the molecular basis of this interaction, we used computational docking. This revealed a preferred conformation in which the C_8-axis of **13** is essentially co-aligned with that of Wza (Supplementary Fig. S15). As a result, and consistent with our experimental results, each sugar residue displays essentially identical interactions with each protein subunit to create a 'grommet-like' binding mode. Consistent with our initial design, both charged groups and sugar hydroxyls create an extensive network of salt bridges and hydrogen bonding. The protonated NH_3^+-6 ammonium, the endocyclic O-5 and the secondary OH-3 groups in **13** interact with Glu-369, Tyr-373 and Arg-372, respectively (Supplementary Fig. S15, Supplementary Discussion).

$Am_8γCD$ 13 blocks Wza under simulated physiological conditions. To evaluate the potential efficacy of $am_8γCD$ **13** upon live *E. coli*, the blockade of Wza was examined at very low transmembrane potentials under conditions resembling the environment in the human gut (that is, at low salt concentrations) at near neutral pH[36–38].

ΔP106-A107 gave the highest unitary conductance in the 2 M KCl buffer and was therefore used for initial tests. Its unitary conductance in 300 mM KCl was 400 ± 10 pS ($n = 3$) at +50 mV (Fig. 2c, bar 7). The interaction of $am_8γCD$ **13** with ΔP106-A107 could be observed at a concentration as low as 20 nM (*trans*) (Fig. 5f). The outer membrane potential at 300 mM KCl for *E. coli* is −7 mV (ref. 39). Blocker binding

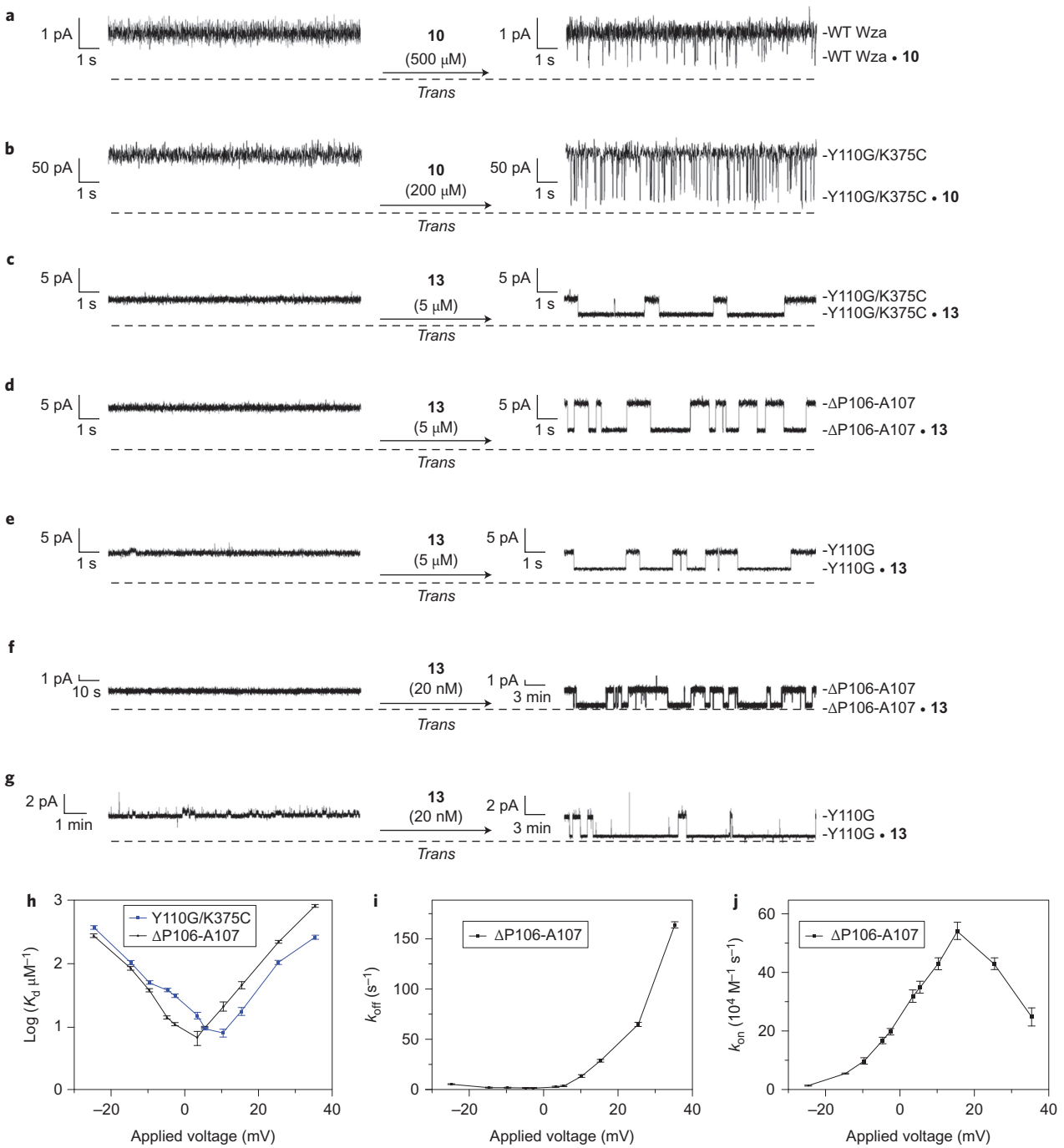

Figure 5 | Interaction of compounds 10 and 13 with Wza mutants. The buffers are 2 M KCl, 5 mM HEPES, 100 μM EDTA, 200 μM DTT, pH 7.5, or 300 mM KCl, 5 mM HEPES, pH 7.5. **a**, Interaction of WT Wza with am$_7$βCD **10** (500 μM, *trans*) at +75 mV in 2 M KCl buffer. **b**, Interaction of Y110G/K375C with am$_7$βCD **10** (200 μM, *trans*) at +75 mV in 2 M KCl buffer. **c**, am$_8$γCD **13** (5 μM, *trans*) binds to Y110G/K375C at +3 mV in 2 M KCl buffer. **d**, am$_8$γCD **13** (5 μM, *trans*) binds to ΔP106-A107 at +3 mV in 2 M KCl buffer. **e**, am$_8$γCD **13** (5 μM, *trans*) binds to Y110G at +3 mV in 2 M KCl buffer. **f**, am$_8$γCD **13** (20 nM) binds to ΔP106-A107 at +5 mV in 300 mM KCl buffer. **g**, am$_8$γCD **13** (20 nM) binds to Y110G at +10 mV in 300 mM KCl buffer. **h**, Dissociation constants (K_d) of Y110G/K375C·**13** (*trans*, $n = 3$) and ΔP106-A107·**13** (*trans*, $n = 3$) versus applied potential in 2 M KCl buffer. The *y*-axis (K_d) is on a logarithmic scale. **i**, k_{off} versus *V* curve for ΔP106-A107 with am$_8$γCD **13** in 2 M KCl buffer. **j**, k_{on} versus *V* curve for ΔP106-A107 with am$_8$γCD **13** in 2 M KCl buffer. Dashed line in **a**–**g**, 0 pA. Mean values (±s.d.) from at least three independent experiments are shown. The sampling rate is 5 kHz.

was therefore also measured at +5 mV, equivalent to −5 mV in *E. coli*. The τ_{off} value (17 ± 4 s) for ΔP106-A107·**13** in 300 mM KCl was much longer than in 2 M KCl (0.33 ± 0.04 s). The K_d for ΔP106-A107·**13** in 300 mM KCl was 44 ± 25 nM (Supplementary Table S3).

Similarly, the unitary conductance of Y110G in 300 mM KCl was 0.30 ± 0.01 nS (+50 mV, $n = 3$), the τ_{off} value for Y110G·**13** was 165 ± 57 s (+10 mV, $n = 3$) and the K_d of Y110G·**13** was 5.6 ± 2.4 nM (+10 mV, $n = 3$, Fig. 5g).

Inhibition of Wza polysaccharide transport in *E. coli*. The ability of blocker am$_8$γCD **13** to bind tightly to the end of Wza that opens into the medium surrounding *E. coli* cells suggested its application as a prospective inhibitor of K30 CPS transport. We tested blocking

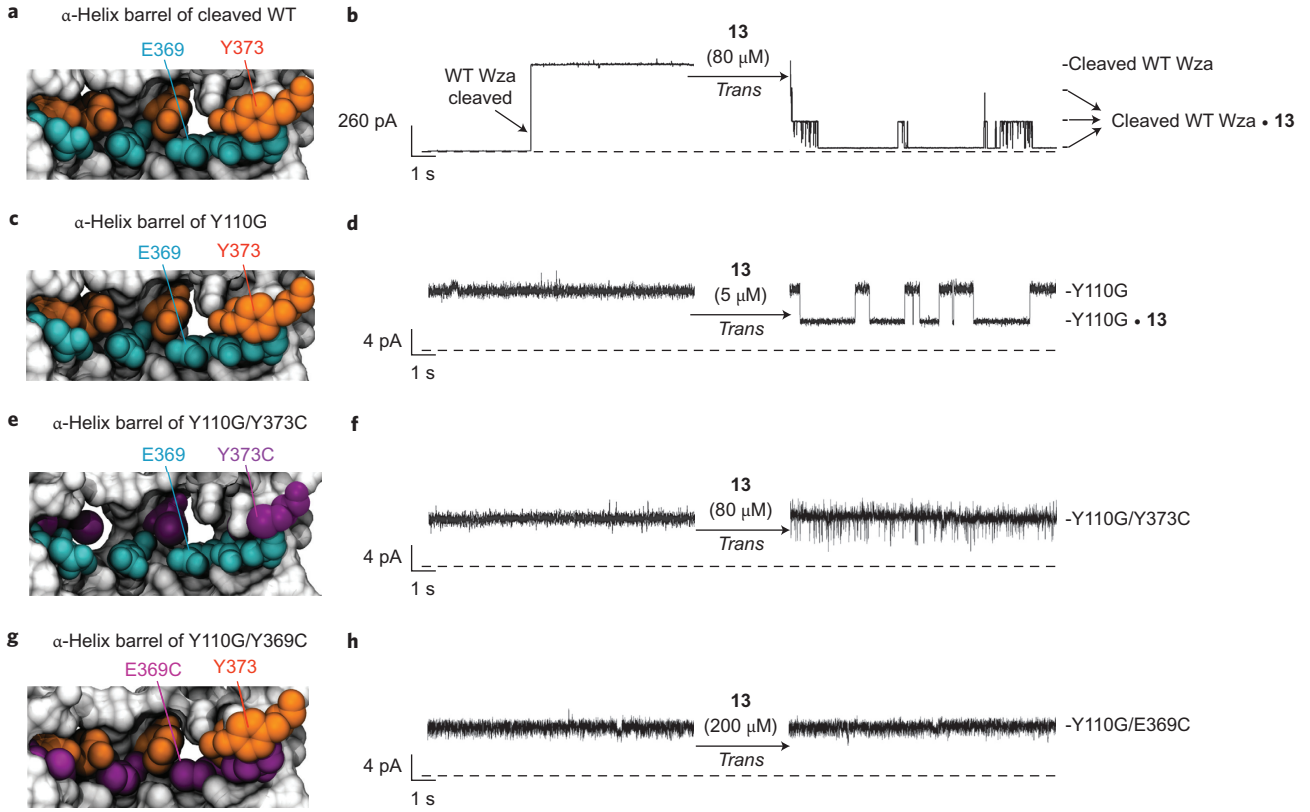

Figure 6 | Interaction of am$_8$γCD 13 with the α-helix barrel of Wza mutants and proteolysed WT Wza. a, The α-helix barrel of WT Wza. **b**, Interaction of am$_8$γCD **13** with proteolysed WT Wza. Proteinase K (10 μl, 20 mg ml^{-1}) was added to the *cis* compartment (1 ml) after a WT Wza pore had inserted into the bilayer. Cleavage was observed at +100 mV in 2 M KCl buffer, as reflected by the sudden jump in current. In 2 M KCl buffer at +100 mV, three levels of blockade are apparent: 502±35 pA (n = 4), 253±30 pA (n = 4) and 19±7 pA (n = 4) (right). **c**, Local structure of the α-helix barrel of mutant Y110G. **d**, The Y110G pore interacts with am$_8$γCD **13** (5 μM) at +3 mV in 2 M KCl buffer. **e**, The α-helix barrel of Y110G/Y373C. **f**, The Y110G/Y373C pore interacts with am$_8$γCD **13** (80 μM) at +3 mV in 2 M KCl buffer. **g**, The α-helix barrel of Y110G/E369C. **h**, The Y110G/E369C channel interacts with am$_8$γCD **13** (200 μM) at +3 mV in the 2 M KCl buffer. Dashed line, 0 pA for **b**,**d**,**f**,**h**. The sampling rate is 5 kHz.

activity on live *E. coli* cells with **13** and also **10** and **3** (Fig. 4), which had proved to be less effective blockers. When pathogenic *E. coli* E69 (O9a:K30:H12), the reference strain for K30 antigen[4,40], was grown in the presence of these molecules, the reduction in CPS expression[41,42] was consistent with the relative abilities to block Wza: in other words, **13** was more active than either **10** or **3** at the same concentrations (Supplementary Fig. S16).

The reduction of K30 polysaccharide on the cell surface[4,12,40] by am$_8$γCD **13** was studied more fully (Fig. 7a), and **13** was found to decrease K30 CPS in a concentration-dependent manner. The molecular mass of the polysaccharide was unchanged at ∼180 kDa (Supplementary Fig. S16), close to the reported value of 150 kDa (ref. 41), suggesting that it is transport and not biosynthesis that is inhibited. The higher inhibitory concentration (IC_{50} = 51±1 μM; Fig. 7b) than the nM affinity we observed in electrical channel recordings could be a consequence of reduced diffusion through the thick barrier of CPS. Interestingly, the level of LPS increased with the decrease in CPS and became saturated at about twice the amount observed in the absence of am$_8$γCD **13** (Fig. 7c).

Exposure of O9a LPS to O9a LPS-specific antibodies. Inhibition of K30 CPS transport in E69 causes defects in the capsule layer[40] that should expose O9a LPS at the cell surface. To test this hypothesis, the attachment of rabbit anti-O9a antibodies[43] was quantified by flow cytometry (FACS)[44] (Supplementary Fig. S20), which revealed a dose-dependent increase in the binding of anti-O9a antibodies[43] (Fig. 7d, bottom) to *E. coli* E69 cells after treatment with am$_8$γCD **13** (Fig. 7d, top) compared with bacteria treated with **3** or **10**, consistent with their relative efficacies in blocking Wza and inhibiting CPS transport (see above). Even at 1 μM, am$_8$γCD **13** caused significant exposure of LPS to LPS-specific antibodies (Fig. 7e).

Complement-mediated killing of bacteria. Normal human serum (NHS) with active complement led to only 15% killing of E69 cells (Fig. 7f, see Supplementary Information, page 10). Consistent with an increased vulnerability in the absence of CPS[44–46], a genetically engineered CPS-minus strain (CWG281, ref. 40) suffered 100% killing in the presence of NHS.

We next tested the killing of bacteria treated with am$_8$γCD **13**. A clear dose response was observed (Fig. 7f, bars 3–11), with up to 84±3% killing of E69 after 1 h at 1 mM. Am$_8$γCD **13** alone had no significant effect on survival in the absence of NHS, implying that killing was complement-mediated and initiated by the ability of am$_8$γCD **13** to weaken the CPS barrier (Fig. 7f, bars 12,13). Deactivated human serum (DHS) led to no killing (Fig. 7f, bar 1).

Defects in CPS will be exacerbated when cells divide in the presence of an inhibitor. After increasing the incubation time to 4 h, 1 mM am$_8$γCD **13** completely killed E69 in the presence of NHS. The concentration of am$_8$γCD **13** required to kill half of the bacteria (EC_{50}) under these conditions was 3.2±0.5 μM (P < 0.006, n = 3).

Discussion

We have shown that functional Wza can be expressed and assembled *in vitro* (Fig. 2a, Supplementary Fig. S2). Because of the considerable bulk of the (periplasmic) extramembraneous domain, bilayer insertion is vectorial (Fig. 2b). Electrical recording

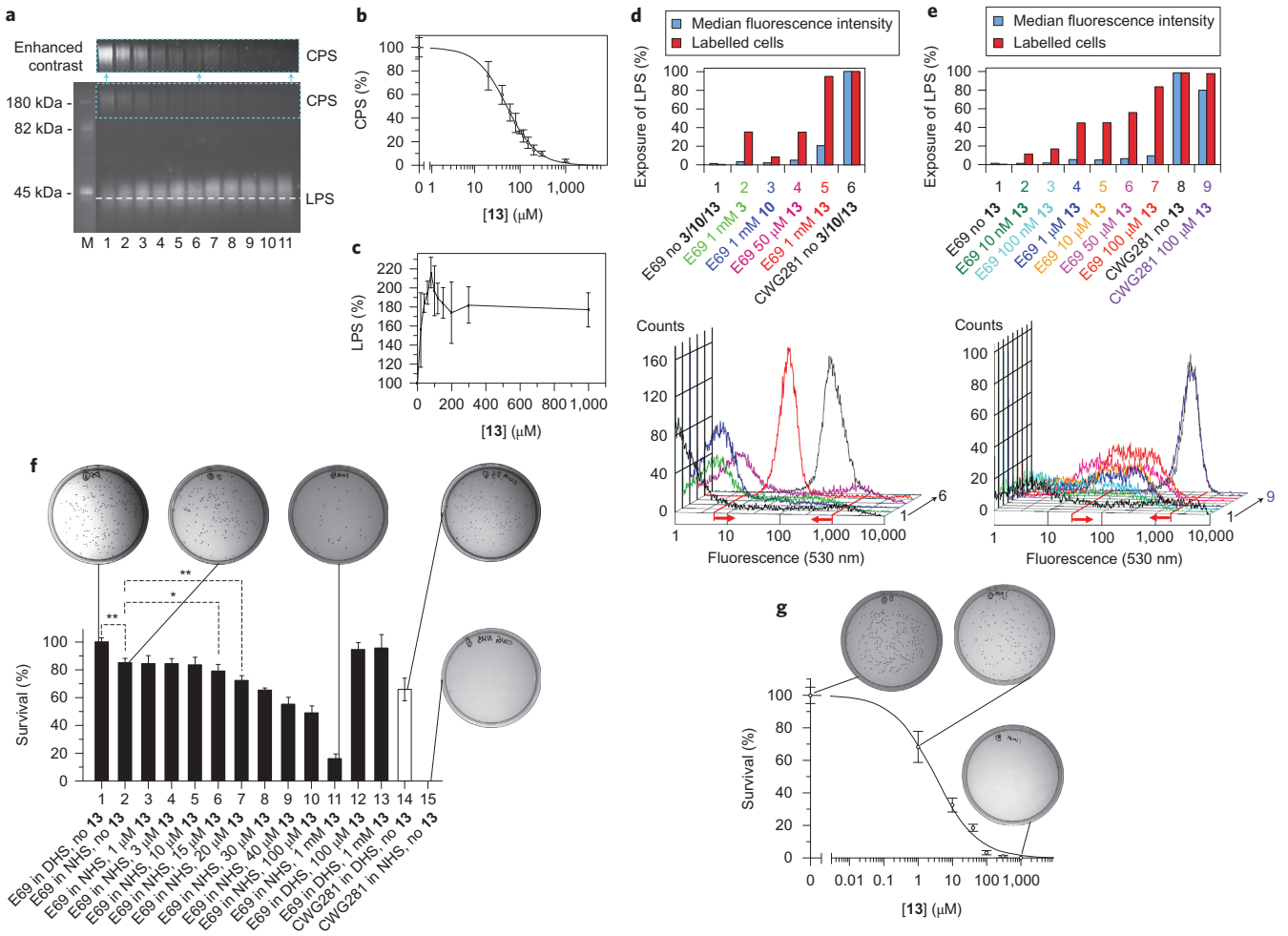

Figure 7 | Effects of am$_8$γCD 13 on K30 CPS and O9a LPS expression in *E. coli* E69, O9a LPS exposure to O9a-specific LPS antibodies and complement-mediated killing of E69. a, Staining of cell extracts of polysaccharides after SDS-PAGE. Lane 1, no treatment with am$_8$γCD **13**; lanes 2–11, after treatment with the concentrations shown in **b** of am$_8$γCD **13**. **b**, Concentration dependence of the effect of am$_8$γCD **13** on K30 CPS synthesis in *E. coli* E69. **c**, Concentration dependence of the effect of am$_8$γCD **13** on LPS synthesis. **d**, Comparison of the binding of anti-O9a antibodies to E69 cells cultured with different Wza inhibitors: am$_6$αCD **3** (green), am$_7$βCD **10** (blue) and am$_8$γCD **13** (purple and red). **e**, Comparison of the binding of anti-O9a antibodies to E69 cells cultured with am$_8$γCD **13** over a range of concentrations. Red arrows in the lower panels of **d**,**e** mark the fluorescence intensity between which cells were considered positively labelled. **f**, Survival of strains E69 (bars 1–13) and CWG281 (bars 14,15) in the presence of NHS or DHS. The samples were incubated at 37 °C for 1 h, RPMI 1640. $^*P < 0.001$; $^{**}P < 0.03$. **g**, Effects of various concentrations of am$_8$γCD **13** on complement-mediated killing of *E. coli* E69. Mean values (±s.d.) from at least three independent experiments are shown.

from open Wza mutants served as a ready, informative, biologically relevant screening method for identifying pore blockers with therapeutic potential, as well as delineating the associated kinetic parameters (that is, k_{on}, k_{off} and hence K_d).

The most potent blocker discovered here, am$_8$γCD **13**, possesses C_8 symmetry, which matches that of its target, and might therefore generate a cooperative binding interaction[20,23]. As shown here, Glu-369, Arg-372 and Tyr-373 in each protein subunit form a previously undiscovered binding site within the α-helix barrel of Wza that spans the outer membrane of *E. coli*. Although our design of a cross-sectional grommet that mimics a sugar helix model (Supplementary Fig. S8) is probably overly simplistic, it is notable that this model predicts a matched left-handed helicity for both K30 CPS and Wza. It suggests too that K30 CPS also adopts a pseudo-C_8 symmetry (with the peripheral GlcA and Galα residues of K30 CPS each engaging every other helix). Therefore, the next generation of blockers could usefully explore a similar 'alternating design' to test this mimicry further.

Under conditions that are close to physiological for *E. coli*, am$_8$γCD **13** blocked the Wza pore with $K_d < 50$ nM. The binding site is accessible from the extracellular environment in intact cells and therefore constitutes an excellent drug target that does not require penetration into the periplasmic space or the interior of the target cell. By contrast, am$_8$γCD **13** was only mildly cytoxic towards a human cell line (HeLa cells) (Supplementary Fig. S21).

Am$_8$γCD **13** is the first effective inhibitor of the translocation of K30 CPS by Wza. Without CPS, pathogenic *E. coli* E69 treated by am$_8$γCD **13** are vulnerable to human complement killing. Protein sequence alignment (Supplementary Table S4) of Wza from *E. coli* E69 (Wza$_{K30}$) with homologues (≥60% identity) revealed another 49 pathogenic bacterial species (mostly Gram-negative, including *E. coli* and *Klebsiella*), comprising 248 pathogenic strains, which share Glu-369 and Tyr-373 or similar residues that have the potential to form salt bridges and/or hydrogen bonds and therefore may also bind am$_8$γCD **13**.

Am$_8$γCD **13** acts as a potentiator of human complement-mediated killing; that is, am$_8$γCD **13** is not itself antibacterial but enhances complement-mediated killing. Accordingly, am$_8$γCD **13** should not be effective outside a host, thereby reducing the possibility of resistance[47]. Its mode of action might also activate additional immune

components. For example, Toll-like-receptor-4 recognizes LPS[48], which is exposed and increased in concentration by the action of 13.

The screening procedure developed here allowed the discovery of a useful lead compound ($am_8\gamma CD$ 13) that is active on live *E. coli* and mediates killing in the presence of complement. The promising activity of 13, through a new mode of action, may therefore be a prototype for a distinctive category of therapeutics against bacteria. Importantly, a similar approach will permit the rapid discovery of a second generation of blockers that anticipate Wza mutations that confer resistance to $am_8\gamma CD$ 13.

Methods

Pore measurements and experiments. For full details see the Supplementary Methods. Conductance measurements were conducted in 5 mM HEPES, 100 μM EDTA, 200 μM DTT, pH 7.5, unless otherwise indicated. Mean inter-event intervals (τ_{on}) were determined over a range of concentrations of blocker, which allowed the determination of k_{on}, the association rate constant for the formation of complexes, over a range of applied potentials. To record under low salt conditions, a single pore was first obtained with 2 M KCl buffer in the bilayer chamber, which was then diluted with water (buffered with 5 mM HEPES at pH 7.5) to 300 mM KCl; below this concentration, currents were typically too low at low potentials to measure reliably. Structures and models of pores were generated with MODELLER[24]. Internal radii along the pore axes were measured by using HOLE[49] (Fig. 1b).

***E. coli* experiments.** For inhibition experiments *E. coli* were grown in the presence of blocker (1 nM, 1 μM and 1 mM). The attachment of rabbit anti-O9a antibodies[43] was quantified by FACS[44] by using secondary fluorescent anti-rabbit antibodies (Supplementary Fig. S20). The difference in fluorescence between the untreated *E. coli* strain E69 (Fig. 7d, bottom, black curve) and the CPS-minus strain CWG281[40] (Fig. 7d, bottom, grey curve) validated this system for measuring LPS exposure. In contrast to its antibacterial activity, $am_8\gamma CD$ 13 was only mildly cytoxic towards a human cell line (HeLa cells) (median lethal dose $LD_{50} = 0.13 \pm 0.02$ mM, $n = 3$, Supplementary Fig. S21).

Received 20 August 2012; accepted 24 May 2013; published online 30 June 2013

References

1. Infectious Diseases Society of America. *Bad Bugs, No Drugs* (IDSA, 2004), available at http://www.fda.gov/ohrms/dockets/dockets/04s0233/04s-0233-c000005-03-IDSA-vol1.pdf.
2. ECDC. *Antimicrobial Resistance Surveillance in Europe*. Annual Report of the European Antimicrobial Resistance Surveillance Network (EARS-Net) (European Centre for Disease Prevention and Control, 2011), available at http://ecdc.europa.eu/en/publications/Publications/antimicrobial-resistance-surveillance-europe-2011.pdf.
3. Lazarev, V. N. & Govorun, V. M. Antimicrobial peptides and their use in medicine. *Appl. Biochem. Microbiol.* **46**, 803–814 (2010).
4. Whitfield, C., Schoenhals, G. & Graham, L. Mutants of *Escherichia coli* O9:K30 with altered synthesis and expression of the capsular K30 antigen. *J. Gen. Microbiol.* **135**, 2589–2599 (1989).
5. Kolkman, M. A., van der Zeijst, B. A. & Nuijten, P. J. Functional analysis of glycosyltransferases encoded by the capsular polysaccharide biosynthesis locus of *Streptococcus pneumoniae* serotype 14. *J. Biol. Chem.* **272**, 19502–19508 (1997).
6. Cuthbertson, L., Mainprize, I. L., Naismith, J. H. & Whitfield, C. Pivotal roles of the outer membrane polysaccharide export and polysaccharide copolymerase protein families in export of extracellular polysaccharides in gram-negative bacteria. *Microbiol. Mol. Biol. Rev.* **73**, 155–177 (2009).
7. Domenico, P., Tomas, J. M., Merino, S., Rubires, X. & Cunha, B. A. Surface antigen exposure by bismuth dimercaprol suppression of *Klebsiella pneumoniae* capsular polysaccharide. *Infect. Immun.* **67**, 664–669 (1999).
8. Wu, C. L. *et al.* Subinhibitory bismuth-thiols reduce virulence of *Pseudomonas aeruginosa*. *Am. J. Respir. Cell. Mol. Biol.* **26**, 731–738 (2002).
9. Howard, C. J. & Glynn, A. A. The virulence for mice of strains of *Escherichia coli* related to the effects of K antigens on their resistance to phagocytosis and killing by complement. *Immunology* **20**, 767–777 (1971).
10. Whitfield, C. Biosynthesis and assembly of capsular polysaccharides in *Escherichia coli*. *Annu. Rev. Biochem.* **75**, 39–68 (2006).
11. Stukalov, O., Korenevsky, A., Beveridge, T. J. & Dutcher, J. R. Use of atomic force microscopy and transmission electron microscopy for correlative studies of bacterial capsules. *Appl. Environ. Microbiol.* **74**, 5457–5465 (2008).
12. Dong, C. *et al.* Wza the translocon for *E. coli* capsular polysaccharides defines a new class of membrane protein. *Nature* **444**, 226–229 (2006).
13. Walker, B., Krishnasastry, M., Zorn, L., Kasianowicz, J. & Bayley, H. Functional expression of the alpha-hemolysin of *Staphylococcus aureus* in intact *Escherichia coli* and in cell lysates. Deletion of five C-terminal amino acids selectively impairs hemolytic activity. *J. Biol. Chem.* **267**, 10902–10909 (1992).
14. Bayley, H. *et al.* Droplet interface bilayers. *Mol. Biosyst.* **4**, 1191–1208 (2008).
15. Collins, R. F. *et al.* The 3D structure of a periplasm-spanning platform required for assembly of group 1 capsular polysaccharides in *Escherichia coli*. *Proc. Natl Acad. Sci. USA* **104**, 2390–2395 (2007).
16. Miles, G., Movileanu, L. & Bayley, H. Subunit composition of a bicomponent toxin: staphylococcal leukocidin forms an octameric transmembrane pore. *Protein Sci.* **11**, 894–902 (2002).
17. Merzlyak, P. G., Capistrano, M. F., Valeva, A., Kasianowicz, J. J. & Krasilnikov, O. V. Conductance and ion selectivity of a mesoscopic protein nanopore probed with cysteine scanning mutagenesis. *Biophys. J.* **89**, 3059–3070 (2005).
18. Stauffer, D. A. & Karlin, A. Electrostatic potential of the acetylcholine binding sites in the nicotinic receptor probed by reactions of binding-site cysteines with charged methanethiosulfonates. *Biochemistry* **33**, 6840–6849 (1994).
19. Karginov, V. A. *et al.* Search for cyclodextrin-based inhibitors of anthrax toxins: synthesis, structural features, and relative activities. *Antimicrob. Agents Chemother.* **50**, 3740–3753 (2006).
20. Banerjee, A. *et al.* Molecular bases of cyclodextrin adapter interactions with engineered protein nanopores. *Proc. Natl Acad. Sci. USA* **107**, 8165–8170 (2010).
21. Nestorovich, E. M., Karginov, V. A., Berezhkovskii, A. M., Parsegian, V. A. & Bezrukov, S. M. Kinetics and thermodynamics of binding reactions as exemplified by anthrax toxin channel blockage with a cationic cyclodextrin derivative. *Proc. Natl Acad. Sci. USA* **109**, 18453–18458 (2012).
22. Gu, L. Q., Cheley, S. & Bayley, H. Capture of a single molecule in a nanocavity. *Science* **291**, 636–640 (2001).
23. Martos, V. *et al.* Calix[4]arene-based conical-shaped ligands for voltage-dependent potassium channels. *Proc. Natl Acad. Sci. USA* **106**, 10482–10486 (2009).
24. Sali, A. & Blundell, T. L. Comparative protein modelling by satisfaction of spatial restraints. *J. Mol. Biol.* **234**, 779–815 (1993).
25. Atkins, E. D. T. & Parker, K. D. Cyclic triad of hydrogen bonds in a helical polymer. *Nature* **220**, 784–785 (1968).
26. Atkins, E. D. T., Parker, K. D. & Preston, R. D. The helical structure of the beta-1,3-Linked xylan in some siphoneous green algae. *Proc. R. Soc. Lond. B* **173**, 209–221 (1969).
27. Gessler, K. *et al.* V-Amylose at atomic resolution: X-ray structure of a cycloamylose with 26 glucose residues (cyclomaltohexaicosaose). *Proc. Natl Acad. Sci. USA* **96**, 4246–4251 (1999).
28. Immel, S. & Lichtenthaler, F. W. The hydrophobic topographies of amylose and its blue iodine complex. *Starch* **52**, 1–8 (2000).
29. Brisson, J. R., Baumann, H., Imberty, A., Perez, S. & Jennings, H. J. Helical epitope of the group B meningococcal alpha(2-8)-linked sialic acid polysaccharide. *Biochemistry* **31**, 4996–5004 (1992).
30. Brisson, J. R. *et al.* NMR and molecular dynamics studies of the conformational epitope of the type III group B Streptococcus capsular polysaccharide and derivatives. *Biochemistry* **36**, 3278–3292 (1997).
31. Kararli, T. T. Comparison of the gastrointestinal anatomy, physiology, and biochemistry of humans and commonly used laboratory animals. *Biopharm. Drug Dispos.* **16**, 351–380 (1995).
32. Nikaido, H. Molecular basis of bacterial outer membrane permeability revisited. *Microbiol. Mol. Biol. Rev.* **67**, 593–656 (2003).
33. Wang, Z. *et al.* Adsorption and desorption of phenanthrene on carbon nanotubes in simulated gastrointestinal fluids. *Environ. Sci. Technol.* **45**, 6018–6024 (2011).
34. Woodhull, A. M. Ionic blockage of sodium channels in nerve. *J. Gen. Physiol.* **61**, 687–708 (1973).
35. Ishihara, K. & Yan, D. H. Low-affinity spermine block mediating outward currents through Kir2.1 and Kir2.2 inward rectifier potassium channels. *J. Physiol.* **583**, 891–908 (2007).
36. Jordt, S. E., Tominaga, M. & Julius, D. Acid potentiation of the capsaicin receptor determined by a key extracellular site. *Proc. Natl Acad. Sci. USA* **97**, 8134–8139 (2000).
37. Jung, K., Veen, M. & Altendorf, K. K^+ and ionic strength directly influence the autophosphorylation activity of the putative turgor sensor KdpD of *Escherichia coli*. *J. Biol. Chem.* **275**, 40142–40147 (2000).
38. Pearl, M., Fishkind, D., Mooseker, M., Keene, D. & Keller, T. III. Studies on the spectrin-like protein from the intestinal brush border, TW 260/240, and characterization of its interaction with the cytoskeleton and actin. *J. Cell Biol.* **98**, 66–78 (1984).
39. Sen, K., Hellman, J. & Nikaido, H. Porin channels in intact cells of *Escherichia coli* are not affected by Donnan potentials across the outer membrane. *J. Biol. Chem.* **263**, 1182–1187 (1988).
40. Drummelsmith, J. & Whitfield, C. Translocation of group 1 capsular polysaccharide to the surface of *Escherichia coli* requires a multimeric complex in the outer membrane. *EMBO J.* **19**, 57–66 (2000).
41. Hungerer, D., Jann, K., Jann, B., Orskov, F. & Orskov, I. Immunochemistry of K antigens of *Escherichia coli*. 4. The K antigen of *E. coli* O9:K30:H12. *Eur. J. Biochem.* **2**, 115–126 (1967).
42. Chakraborty, A. K., Friebolin, H. & Stirm, S. Primary structure of the *Escherichia coli* serotype K30 capsular polysaccharide. *J. Bacteriol.* **141**, 971–972 (1980).
43. Clarke, B. R., Cuthbertson, L. & Whitfield, C. Nonreducing terminal modifications determine the chain length of polymannose O antigens of *Escherichia coli* and couple chain termination to polymer export via an ATP-binding cassette transporter. *J. Biol. Chem.* **279**, 35709–35718 (2004).

44. Fernandez-Prada, C. M. *et al.* Deletion of wboA enhances activation of the lectin pathway of complement in *Brucella abortus* and *Brucella melitensis*. *Infect. Immun.* **69**, 4407–4416 (2001).
45. Moranta, D. *et al.* *Klebsiella pneumoniae* capsule polysaccharide impedes the expression of beta-defensins by airway epithelial cells. *Infect. Immun.* **78**, 1135–1146 (2010).
46. Regueiro, V. *et al.* *Klebsiella pneumoniae* increases the levels of Toll-like receptors 2 and 4 in human airway epithelial cells. *Infect. Immun.* **77**, 714–724 (2009).
47. Smith, P. A. & Romesberg, F. E. Combating bacteria and drug resistance by inhibiting mechanisms of persistence and adaptation. *Nature Chem. Biol.* **3**, 549–556 (2007).
48. Lebeer, S., Vanderleyden, J. & De Keersmaecker, S. C. Host interactions of probiotic bacterial surface molecules: comparison with commensals and pathogens. *Nature Rev. Microbiol.* **8**, 171–184 (2010).
49. Smart, O. S., Goodfellow, J. M. & Wallace, B. A. The pore dimensions of gramicidin A. *Biophys. J.* **65**, 2455–2460 (1993).
50. Humphrey, W., Dalke, A. & Schulten, K. VMD: visual molecular dynamics. *J. Mol. Graph.* **14**, 33–38, 27–28 (1996).

Acknowledgements

The authors thank J. Naismith and G. Hageluken for the pWQ126 (pBAD-Wza) plasmid, WT Wza protein and the E69 strain, C. Whitfield for the CWG281 strain and O9a antiserum, and N. Rust, C.M. Tang and Min Chen for discussions and advice. The authors thank the Medical Research Council and the Engineering and Physical Sciences Research Council for financial support. L.K. received a Wellcome Trust Value in People (VIP) award and a UK/China Postgraduate Research Scholarship. L.H. was supported by a Biotechnology and Biological Sciences Research Council studentship. B.G.D. is a Royal Society Wolfson Research Merit Award recipient.

Author contributions

L.K., S.C., B.G.D. and H.B. designed the experiments. L.K. performed protein engineering, single-channel recording, molecular modelling, microbiology, cell wall extraction, flow cytometry, complement-mediated killing and cytotoxicity experiments. Q.L. performed protein engineering. L.H. performed molecular modelling. L.K., B.G.D. and H.B. analysed results. L.K., B.G.D. and H.B. wrote the paper.

Additional information

Supplementary information and chemical compound information are available in the online version of the paper. Reprints and permissions information is available online at www.nature.com/reprints. Correspondence and requests for materials should be addressed to B.G.D. and H.B.

Competing financial interests

A patent has been filed by the University of Oxford and, if licensed, will afford authors fees and royalties in the manner set down by the University.